Temperature driven transformations of glycine molecules embedded in interstellar ice

Maysá Yusef Buey, Tzonka Mineva, Dahbia Talbi, Mathias Rapacioli

Temperature driven transformations of glycine molecules embedded in interstellar ice †

Maysa Yusef Buey,[a] Tzonka Mineva, [b] Dahbia Talbi, [c] and Mathias Rapacioli* [d]

Formation of glycine aminoacid on ice grains in space raises fundamental questions about glycine chemistry in interstellar media. In this work, we studied glycine conformational space and the related tautomerization mechanisms in water media by means of QM/MM molecular dynamics simulations of four glycine conformational isomers (*cc*, *ct*, *tc*, *tt*). Interstellar low density amorphous (LDA) ice and T = 20 K were considered as representative for cold interstellar ice environment, while temperatures of 250 and 450 K were included to model rapid local heating in the ice. In addition to LDA environment, water clusters with 4, 17, and 27 H_2O molecules were subjected to QM/MM dynamics simulations that allowed to evaluate glycine tautomerization behaviour in water surface-like environments. The tautomerization processes were found strongly dependent on the number of water molecules and specific isomer structure. All the glycine isomers preserve their canonical "neutral" conformations in interstellar conditions.

1 Introduction

There is more and more evidence that the formation of glycine, the simplest amino acid, could occur in space. Indeed, it has been discovered in the Murchison meteorite[1], detected in samples of cometary dust from comet 81P/Wild 2 returned by the Stardust mission[2], observed in the coma of the Churyumov- Gerasimenko comet by the ROSINA mass spectrometer[3] and very recently detected in the Ryugu samples collected by the Hayabusa2 mission[4]. Gas-phase glycine has been widely searched in interstellar sources[5]. A first detection was claimed in 2003[6] but it was refuted in 2005[7] and up to now, glycine has not been detected in the interstelar medium (ISM). From the standpoint of astrochemical modelling, the formation of glycine in space has been investigated considering both gas phase[8] and solid state chemistry[9] and have demonstrated the need for a water ice mediated mechanism for glycine to form in space.

In the laboratory, many studies on glycine in gas phase or embedded in pure or mixed water ices as models of interstellar ices have been undertaken. Most of them were devoted to either the formation of glycine or to its stability with respect to external sources of radiation[10–18], but only few of them focused on the conformations of the formed glycine[13,16,19].

Glycine is known to exists in two forms: the canonical "neutral" NH_2CH_2COOH (hereafter called neutral and labelled N-Gly) and the zwitterionic $NH_3{}^+CH_2COO^-$ (hereafter labelled as Z-Gly). We note that canonical "neutral" and "zwitterionic" isomers are both neutral molecules. The word "neutral" is rather used to distinguish the neutral amine and carboxylic groups in the canonical isomer from the respective charged groups in the zwitterionic isomer. The N-Gly is stable in gas-phase or in low temperature inert matrices[19,20] while the Z-Gly, is stable in water solution or in glycine crystals. Following the work of Maté *et al.*[19], the transformation from neutral to zwitterionic glycine is restricted in non-polar environment, whereas the embedding of neutral glycine in polar (water) medium favors its conversion to Z-Gly even at low temperature of 25K[19]. Holtom *et al.*[13] reported on the formation of zwitterionic glycine ($CH_3{}^+NHCOO^-$) in methylamine–carbon dioxide ices at T=10K and anionic isomers ($NH_2CH_2COO^-$) upon heating to 300K and cooling down to 10K. In a more recent study[16], the formation of N-Gly in a water-rich ice at 13K without external energetic stimuli has been confirmed by in-situ reflection absorption infrared (RAIR) spectroscopy. Furthermore, upon heating to 230 - 240K N-Gly converted only partially to its Z-Gly form. These different transformation behaviours of glycine in water-rich icy environment at low temperature could, therefore, depend not only on the specific ice composition and temperature[19], but also on the formation mechanism that may preferentially stabilise particular glycine conformer(s) over others.

Neutral glycine conformers in gas-phase are defined with respect to the three internal rotational degrees of freedom around glycine C-C, C-O and C-N bonds, resulting in eight conformers[21]. Among them the lowest in energy is the trans-trans-trans (*ttt*) conformer[22] followed by the second most stable cis-cis-cis (*ccc*) conformer, higher in energy by only 1.4 kcal/mol than the ttt conformer[23]. In water medium and at room temperature, the small relative energy difference between the conformers is overcome resulting in an ensemble of conformations[24].

The relative energy stability and the mechanism of tautomerization from neutral to zwitterionic conformers have been pre-

[a] *Laboratoire de Chimie et Physique Quantique (LCPQ/FERMI), UMR5626, Université de Toulouse (UPS) and CNRS, 118 Route de Narbonne, F-31062 Toulouse, France*
[b] *ICGM, Univ. Montpellier, CNRS, ENSCM, Montpellier,France; E-mail : tzonka.mineva@enscm.fr*
[c] *LUPM, Univ. Montpellier, CNRS, Montpellier, France; E-mail : dahbia.talbi@umontpellier.fr*
[d] *Laboratoire de Chimie et Physique Quantique (LCPQ/FERMI), UMR5626, Université de Toulouse (UPS) and CNRS, 118 Route de Narbonne, F-31062 Toulouse, France; E-mail: mathias.rapacioli@irsamc.ups-tlse.fr*

dominantly investigated by quantum mechanics (QM) chemical methods, including Hartree-Fock, density-functional theory (DFT), and wave function methods (MP2, CCSD)[21,24–33] as well as QM coupled to molecular mechanics (QM/MM) approaches[26,34–36]. The water environment was modeled either as a continuum solvent model[31] or by explicitly considering small water clusters (from one to ten H_2O molecules)[25,30,33,37], or as periodic boxes[24,29]. All the studies agreed that water environment stabilises the Z-Gly conformer, but disagree on the water-glycine interactions that favor the zwitterionic form. One water molecule and excess of one electron were found sufficient for N-Gly to Z-Gly tautomerization[30], whereas in mono- and dihydrated clusters only N-Gly was identified[25]. Molecular Dynamics (MD) simulations within the Car-Parinello scheme on zwitterionic glycine in a water box resulted in 4.4 water molecules in the first solvation shell[29]. The existence of numerous local minima were found by Bachrach *et al.*[37] in their DFT study on the potential energy surface of glycine-$(H_2O)_7$ cluster. The authors identified thirty-five N-Gly and sixty-one Z-Gly minimum-energy conformations under water influence. This suggests that a statistical averaging of glycine conformations is needed to describe the micro-properties of glycine-water systems. The stabilization of N-Gly in water solvent (*ttc* and *gtc*) in comparison to N-Gly in gas-phase, is obtained from QM/MM-MD simulations at T=300K[34], therefore emphasising the role of explicit water molecules in the models.

The theoretical studies remain also inconclusive about the mechanism of N-Gly to Z-Gly tautomerization in water. An intramolecular H-transfer (direct mechanism) is concluded mainly in these studies, which treated exclusively N-Gly conformer with cis orientation between the amine and carboxyl group (*ccc* or *cct*)[25,27,31,38,39], a suitable glycine configuration for a facile direct H-transfer. Only few works report on a water-assisted tautomerization that involves one or few molecules in the H-transfer mechanism[34,37]. These results are predominantly obtained if trans orientation between amine and carboxyl were present among the studied conformers. A long-term sampling in the order of 0.5 to 1 ns has been achieved with classical MD simulations, based on empirical force fields[38,40], including a reactive force-field[24]. Despite the longer sampling, feasible with classical MD simulations, the lack of polarization on the MM-atoms in the non-polarizable and non-reactive force-fields was established insufficient to reproduce correctly enthalpy and entropy ratio in the tautomerization free energy.[24,38].

Nevertheless the theoretical works contributed valuable advances on the stability and tautomerization of glycine conformations in water medium, the accumulated knowledge is still incomplete. Moreover, it does not apply directly to the glycine conformational behaviour in the interstellar ice media. Hitherto, glycine tautomerization has been studied exclusively in view of its biological relevance at room temperature[24,29,34,38,40].

In this work, we address the questions of glycine conformational space and the related transformations, including tautomerization mechanisms, in water media at three temperatures, namely 20 K mimicking the cold interstellar space conditions and 250 and 450 K in order to model the possible rapid heating processes of ices caused by cosmic rays or stellar winds matter fluxes[41]. We also note that 20 and 250 K temperatures were chosen in accordance to the experimental conditions, used in the investigation of glycine formation by Ioppolo *et al.*[16] (13 - 240 K) and by Maté *et al.*[19] (25 - 200 K).

We considered four glycine conformers, each of them in four different orientations, embedded in water as supra-molecular models. Water clusters of increasing sizes were studied: from n_{H_2O}=4, 17, 27 to a representative model (of about 350 H_2O molecules) of a Low Density Amorphous (LDA) interstellar ice. For these purpose, local optimizations and molecular dynamics studies were performed using DFT and DFT(QM)/MM hybrid approaches.

2 Method and General Strategy

In the following two sections, we first provide computational details regarding the potential energy calculation and molecular dynamics before presenting the strategy followed to build the different N-Gly-water models.

2.1 Computational details

All calculations were performed using the deMon2k code[42]. If not stated otherwise, the DFT calculations were carried out with DZVP basis set[43], as well as the automatically generated auxiliary basis set GEN-A2*[44] in combination with the PBE96 exchange-correlation functional[45]. The choice of the exchange-correlation functional was determined from previous theoretical studies where the PBE functional was shown to provide a fair description of glycine molecular systems[19,46,47]. The Restricted Kohn-Sham (RKS) SCF tolerance was set tighten between 10^{-6} and 10^{-9} a.u. In addition, dispersion corrections were added to the electronic energy through empirical C_6 coefficients[48].

DFT/MM hybrid calculations have also been performed, within the electronic embedding incode additive QM/MM scheme in deMon2k[49]. The DFT region was treated as mentioned above and the MM region was described by the AMBER-FF99SB force field potential (TIP3P for water molecules)[50–53] which includes the Coulomb effects inside the MM part. QM-MM and MM interactions are described by the Lennard-Jonnes potential and Coulomb interactions between MM point charges atoms and QM electronic densities are considered, thus capturing the polarization of the QM region by the MM environment.

Local geometry optimisation calculations were performed with the Broyden, Fletcher, Goldfarb, Shanno (BFGS)[54–57] Hessian update scheme, with a maximum root mean square (RMSQ) forces tolerance of 10^{-4} a.u. Born-Oppenheimer Molecular Dynamics (BOMD) were performed in the canonical ensemble. Each trajectory length equals to 10ps, with few exceptions noted in the Results Section. The integration time step was set to 1 fs. Linear and angular momentum conservation were forced with a tolerance value of 10^{-8} a.u. The temperatures were maintained by a chain of 5 Nose Hoover thermostats[58–60] with energy exchange frequency of 800 cm^{-1}. The BOMD simulations were carried out at three temperatures of 20, 250 and 450 K.

2.2 Initial Molecular Structures: N-Gly Isomers, LDA ice model and water clusters

2.2.1 N-Gly Conformational Isomers

Eight most stable N-Gly isomers in gas phase were identified from CCSD(T) energy calculations on the conformers geometries, optimized with DFT[21]. In this set of glycine conformers the orientation of the carboxylic hydrogen with respect to N atom was considered. For the purpose of our work, only four out of the reported eight isomers were chosen, disregarding the rotation around C-N bond. It represents various rotations of the -COOH group around the C-C bond and rotation of the carboxylic hydrogen as shown in Figure 1. The four conformational isomers are defined by two dihedral angles, noted as α (N-C-C-O) and β (C-C-O-H). In Figure 1, the relative energies for each isomer, in gas-phase, are reported. These values were obtained from the geometry optimization using aug-cc-PVTZ basis.

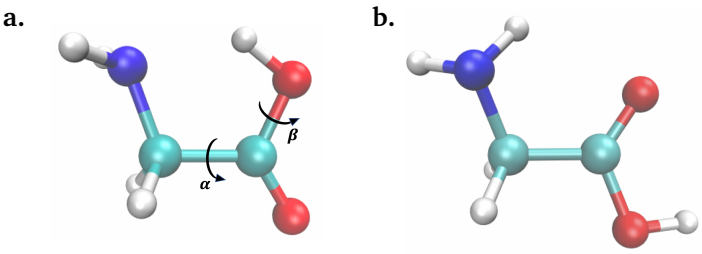

cis-cis(*cc*)-N-Gly
$\alpha \sim [6°]$ $\beta \sim [-1.5°]$
$E_R = 0.0$ kcal.mol^{-1}

trans-trans(*tt*)-N-Gly
$\alpha \sim [162°]$ $\beta \sim [177°]$
$E_R = 2.6$ kcal.mol^{-1}

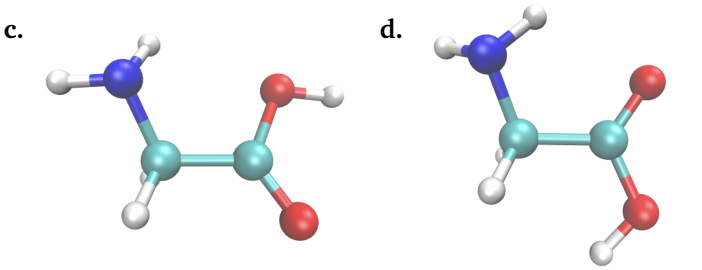

cis-trans(*ct*)-N-Gly
$\alpha \sim [-30°]$ $\beta \sim [-178°]$
$E_R = 4.0$ kcal.mol^{-1}

trans-cis(*tc*)-N-Gly
$\alpha \sim [166°]$ $\beta \sim [-2.5°]$
$E_R = 7.5$ kcal.mol^{-1}

Fig. 1 DFT optimized neutral glycine (N-Gly) isomers. Cis and trans conformational character described by the α and β dihedral angles.

In the following, the neutral glycine conformers will be denoted as *xy*-N-Gly, where *x* and *y* label the cis (*c*) or trans (*t*) conformer. *cc*-N-Gly (Figure 1-a) refers to the neutral glycine isomer with $|\alpha|$ and $|\beta|$ angles close to 0° and *tt*-N-Gly (Figure 1-b) corresponds to a neutral glycine isomer with $|\alpha|$ and $|\beta|$ values close to 180°. In the two remaining isomers, α and β have different cis or trans orientations leading to *ct*-N-Gly (Figure 1-c) and *tc*-N-Gly (Figure 1-d) isomers.

Geometry optimization of the Z-Gly conformers in gas-phase were carried out. As expected, the Z-Gly conformers transformed to N-Gly minimum energy structures during the local geometry optimization.

2.2.2 N-Gly isomers trapped in LDA ice

In order to model the interstellar ices, we have used the Low Density Amorphous (LDA) ice model from Ghesquière *et al.*[61]. It consists of 352 water molecules, equilibrated previously from MD simulations[62]. Water molecules were described by TIP4P potential with an NPT ensemble to control the temperature and pressure of the interstellar ice conditions and the density of water was monitored to be approximately 0.958 g/cm^3. More details can be found in ref.[61]. Figure 2 shows this LDA ice model used in the present study with 20 Å cubic box dimensions. Each of the four minimum energy N-Gly isomers, described in Section 2.2.1 (Figure 1) was introduced into the LDA ice model. The N-Gly molecule was first positioned at the center of mass of the LDA ice model. Second, the closest 8 or 9 water molecules surrounding the N-Gly isomer, were deleted to maintain a minimal distance of 2 Å between the N-Gly and water atoms. This criteria was established in order to avoid any convergence issue in the subsequent dynamical simulations. To further increase the sampling we displaced the center of mass of *xy*-N-Gly with respect to the center of mass of LDA ice model and reoriented each *xy*-N-Gly isomer randomly in four different positions. We therefore generated four different water neighbourhoods around every glycine isomer, resulting in sixteen *xy*-N-Gly-LDA ice systems.

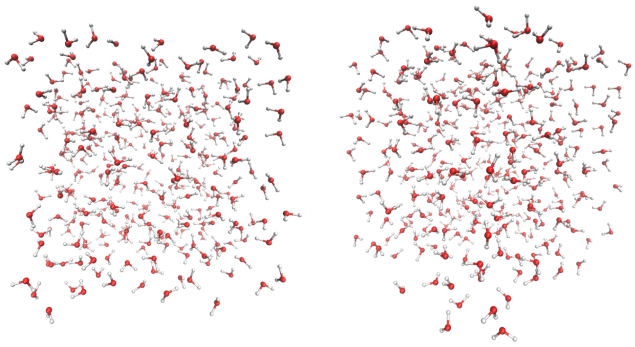

Fig. 2 Top (left) and side (right) view of the LDA ice model from Ghesquière *et al.*[61]. This ice model was used (with no modifications) as a bulk structure for all *xy*-N-Gly embedded systems investigated in this work.

The QM-MM border was defined by a sphere with a radius $R_{cut-off} = 8.5$ Å and an origin at the center of mass. Doing so, the *xy*-N-Gly and its several first solvation shells, containing 61-62 water molecules, were treated at the DFT level, while the remaining 282-283 water molecules were described at the MM level (see Section 2.1).

The structures were first optimized leading to a total of sixteen stable *xy*-N-Gly-LDA ice models (four per neutral glycine isomer), used as starting structures for the BOMD/MD simulations. As a representative example, Figure 3-a reports a snapshot of LDA-embedded *cc*-N-Gly. Note that at temperatures higher than 170K, the LDA ice organization is not maintained, with possible water

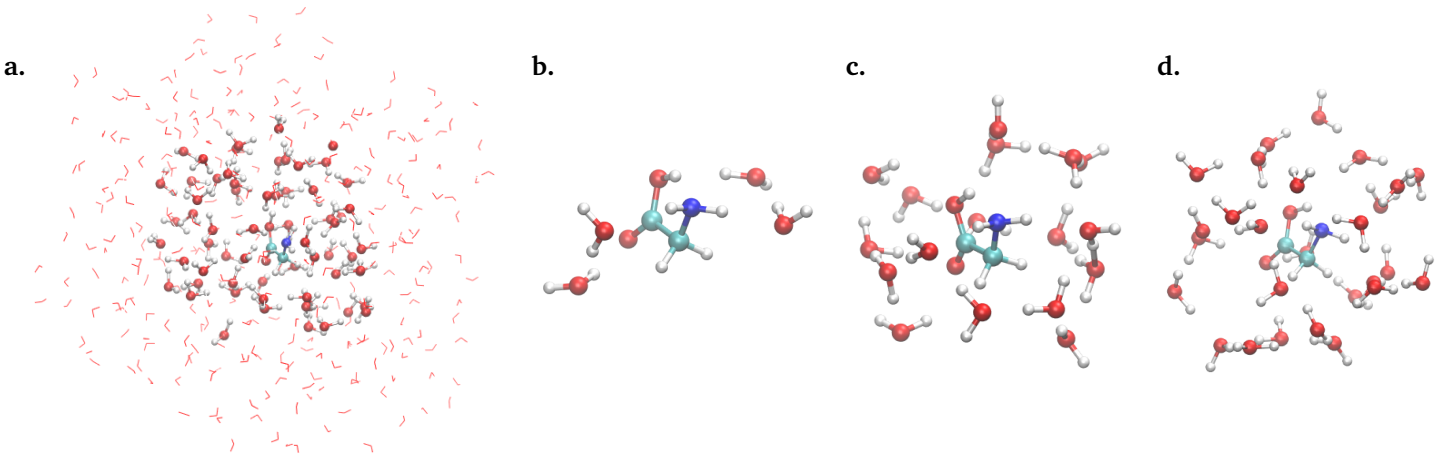

Fig. 3 Representative snapshots of the four different N-Gly embedded molecular systems extracted from the BOMD simulations. The atoms, treated at DFT level are shown as balls and those at MM level as lines. a) *cc*-Gly- 61 H_2O(QM)-282 H_2O(MM) model; b) *cc*-Gly- 4H_2O cluster; c) *cc*-Gly-17H_2O cluster. d)*cc*-Gly- 27H_2O cluster.

desorption[61,63]. For an easier reading, we keep the "LDA" label for the simulations at T = 250 and 450 K.

2.2.3 Water Cluster

If the chemical evolution of glycine mostly results from the interactions with the closest molecules (first solvation shell), the dynamical evolution of the latter also depends on the water molecules further from the glycine. In order to characterize this effect, we have performed simulations in smaller water environments. They do not correspond to the most stable cluster structures (as in the previous works[24,25,64,65]).

For each isomer, glycine was introduced inside the ice model as described in the previous section with four various random displacements/orientations and the clusters were built by selecting only the glycine molecule and its n (4, 17 or 27) closest surrounding water molecules. The largest distance between glycine and water atoms are within 4.5, 6 and 7 Å for the clusters with n=4, 17 or 27 water molecules, respectively.

For these clusters, all atoms were treated at the DFT level. The geometry optimizations were not carried out at variance in the case of *xy*-N-Gly -LDA ice models in order to maintain the original random reorientations of *xy*-N-Gly isomers inside the water clusters. These *xy*-N-Gly-$n$$H_2O$ initial structures allowed to generate 144 BOMD trajectories (3 water cluster sizes; 4 random positions/orientations, 4 conformational N-Gly isomers and 3 temperatures) of 10ps. Some snapshots taken from these MD are exemplified in Figure 3 b, c, and d.

3 Results

In the course of the performed dynamics trajectories, a number of reshaping of the glycine molecule were observed. It involves conformerisation between the different N-Gly forms, tautomerization toward a zwitterionic form, as well as the partial or total loss of an hydrogen atom leading to ionic compounds. In the next Section 3.1, we present and discuss the observed glycine conformational isomers and their ionized forms and a detailed description of reaction pathways is provided. In Section 3.2, a deeper quantitative analysis is performed to discuss the role of the water environment size and of the temperature on the glycine evolution.

3.1 Glycine conformers and reaction path analysis

3.1.1 Neutral conformers

The dynamical evolution of neutral glycine is tracked by the evolution of the two dihedral α and β angles (see Section 2.2.1). The changes of α and β along selected trajectories are exemplified in Figure 4. For instance on the left panels, it is shown that at 20K, α and β dihedral angles remained almost invariant with respect to their initial values. The obtained small values of their standard deviations, reported in Table 1, confirm that the nature of the initial *xy*-N-Gly isomers are preserved along these dynamics.

xy-N-Gly	$\alpha(^\circ)$	$\beta(^\circ)$
cc	5.3 ± 3.5	5.5 ± 3.0
ct	28.7 ± 11.1	167.1 ± 4.0
tt	157.8 ± 4.7	162.4 ± 6.6
tc	173.5 ± 3.7	8.9 ± 4.7
tt-Rotamer	113.8 ± 6.5	176.3 ± 2.4

Table 1 Average absolute values for α and β dihedral angles and standard deviations for five selected trajectories (*cc*- *ct*- *tc*-and *tt*-N-Gly-27H_2O at T=20K).

On the other hand, Figure 4-right panels illustrate the transformation of N-Gly molecule from one isomer to another one. Such transformations were only observed for initial geometries involving either *ct*-N-Gly or *tc*-N-Gly isomers. All conformerisations observed for the *ct*-N-Gly isomer, turned toward the *tt*-N-Gly one.

Those observed for *tc*-N-Gly isomer resulted into *cc*-N-Gly one. These trends in isomers conformerisation are consistent with the fact that *cc*-N-Gly and *tt*-N-Gly are the most energetically stable forms of neutral glycine in gas phase and in water[34]. In addition, rotations around the C-C bond (*ct*-N-Gly → *tt*-N-Gly and *tc*-N-Gly → *cc*-N-Gly) appear to be to be more favourable than those around the C-O bond (*ct*-N-Gly → *cc*-N-Gly and *tc*-N-Gly → *tt*-N-Gly), which is consistent with the higher rotational barriers around the C-O bond than those around the C-C bond, computed at MP2[34] and CPCM-CCSDT[66] levels of theory.

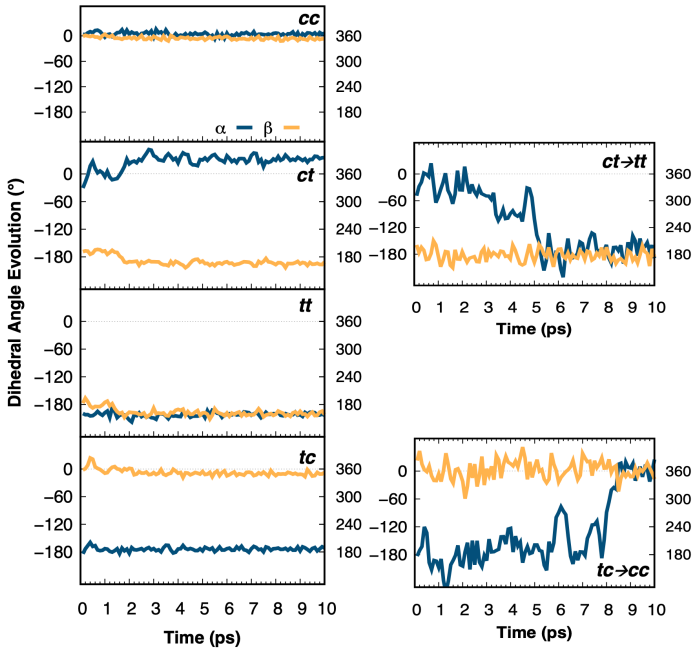

Fig. 4 Left panels illustrate the monitored α and β dihedral angles for four *cc*- *ct*- *tc*-and *tt*-N-Gly-27H_2O molecular systems (dynamics at T=20K). On right panels, the isomer conformerisation for both *ct*- and *tc*-N-Gly-17H_2O molecular systems are captured (dynamics at T=450K). A modulus of 2π was applied for angle values larger than 70°.

Interestingly, a new geometry of neutral glycine (hereafter called rotamer form), unstable in gas phase, was observed during some trajectories. It corresponds to a rotation of the -OOH group around the C-C bond as shown in Figure 5-upper-left panel where the plane defined by the C-C bond and the nitrogen atom and the one defined by the same C-C bond and the carboxylic group of glycine are getting closer to orthogonality (more precisely $|\alpha| \sim 75°$).

We note that this rotamer configuration appeared in some trajectories initiated from *cc*- *ct*- *tc*- or *tt*-N-Gly initial glycine isomers. In Figure 6, an example for rotamer formation from the *tt*-N-Gly isomer form is tracked from the evolution of α and β angles. It demonstrates that β dihedral angle oscillates around $\pm 180°$, thus indicating *trans* conformer, whereas the α dihedral angle shifted by $\sim 60°$. Similar conformational rotamers were attributed to transition state structures in the isomerization reactions of neutral glycine in water, studied with QM/MM umbrella sampling simulations at T = 300K[34]. Without fixing the degrees of freedom, our simulations revealed that these rotamers occur

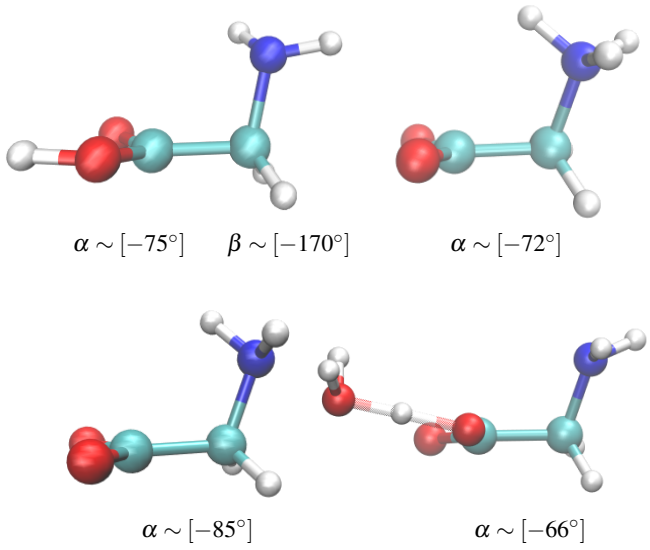

Fig. 5 Rotamer conformers, and corresponding α and β angles, for neutral (upper-left panel), zwitterion (upper-right panel), anion (lower-left panel) and proton delocalized (lower-right panel) glycine forms.

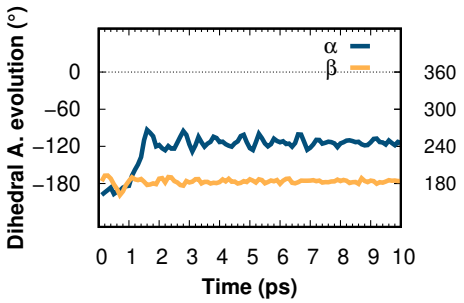

Fig. 6 α and β dihedral angles dynamics evolution for the *tt*-N-Gly-27H_2O rotamer (dynamics at T=20K). A modulus of 2π was applied for angle values larger than 70°.

not only for the neutral but also, as will be seen below, for the zwitterionic and anionic forms of the glycine-water systems (see below and Figure 5), even in small water clusters with n=17 and 27 molecules.

3.1.2 Zwitterion isomers

The zwitterionic glycine (Z-Gly) is another form of glycine molecule with a net neutral charge that has two charged functional groups (one positive and one negative). With respect to N-Gly, the zwitterionic form of glycine is characterized by the abstraction of proton from its carboxylic group and the hydrogenation of its amino group (see Figure 7-top,left). The observation of Z-Gly during dynamics is a direct result of its stabilisation by the surrounding water molecules, since this form is unstable in gas phase as reported in Section 2.2. This form is particularly interesting as it is the most natural form of glycine reported in the literature in aqueous solution at room temperature or under the form of crystals[67,68].

The dynamic evolution from N-Gly to Z-Gly molecular systems,

appeared to be possible for any initial N-Gly isomer, excluding the *tt*-N-Gly. This can be related to the fact that *tt*-N-Gly isomer registers the largest distance between the proton (associated to the carboxylic group) and the nitrogen atom in glycine. In addition, from the energetic point of view, *tt*-N-Gly is particularly stable in gas phase.

As will be detailed in Section 3.2, the formation of Z-Gly is found to be more favourable when the initial N-Gly geometry corresponds to the *cc* isomer. This can be explained due to the proximity between the hydrogen atom attached to the carboxilic group and the nitrogen atom in the amino group. Indeed, almost all the observed Z-Gly forms resulted from a direct proton transfer, where the carboxylic proton shifts toward the amino group in agreement with previous studies on the tautomerization mechanism of glycine[25,27,31,36,38]. In Figure 8-top left, the direct proton transfer reaction path (N-Gly $\rightarrow$ Z_D-Gly) is illustrated by the evolution of distances N-$H_{1,2,3}$ and O-$H_{3,X}$ where H_1 and H_2 are the hydrogen atoms initially bonded to nitrogen, H_3 is the hydrogen atom initially involved in the carboxylic group and H_X is, at a given time, the closest hydrogen to any of the glycine oxygen atoms (O_g-H_X) or to the glycine nitrogen atom (N-H_X). We note the rapid transformation from N-Gly to Z_D-Gly that is observed only after 0.5ps.

Figure 8(top right) captures another type of proton transfer detected in the dynamics where the carboxilic proton migrates throughout the water molecules surrounding the glycine molecule. This concerted proton transfer was mostly observed with initial *ct*- and *tc*-N-Gly isomers and allowed to overpass the large distances between the two functional groups in these isomers. Only two concerted proton transfer mechanism were observed for initial *cc*-N-Gly isomers, out of the total of 29 Z-Gly forms registered. Figure 8-(top right) shows the longer transfer's life time for the concerted proton transfer mechanisms with respect to the direct one. Indeed, the first proton transfer from the carboxylic group to one water molecule occurs at around 0.8ps, followed by 2ps of dynamics where the proton migrates through different surrounding water molecules. Finally, a new bond between a proton from other H_2O molecule is formed with the nitrogen atom, terminating the transformation from N-Gly $\rightarrow$ Z_C-Gly (after $\sim$2.6ps dynamics).

Let us finally mention that a rotamer Z-Gly form was also identified (see Figure 5 top-right) with perpendicular carboxylic / nitrogen plans, similarly to the previously reported N-Gly rotamer cases.

3.1.3 Anionic forms

In some trajectories, a negatively charged glycine form was observed, namely a dehydrogenated glycine molecule resulting from the loss of the proton of the carboxylic group (see Figure 7-top right). These forms were observed in trajectories with *tc*-, *ct*- and *tt*-N-Gly initial isomers, but not in those starting from the *cc*-N-Gly isomer. This can be explained from the proximity between the amino and carboxilic groups in *cc*-N-Gly isomer, leading to a direct proton transfer between these functional groups rather than the proton loss (see Section 3.1.2). On the other hand, for *tc*- *ct*- and *tt*-N-Gly isomers, other mechanisms involving water

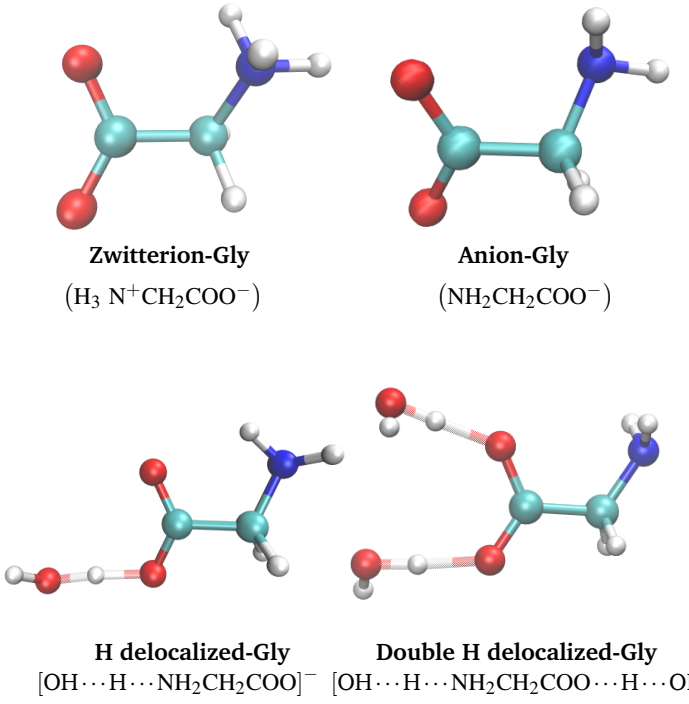

Fig. 7 Illustration of four different glycine forms observed along dynamics: zwitterion glycine (top-left panel), anion (top-right panel) and one and two proton delocalization forms of glycine (bottom-left and right panels).

molecules are favoured. The already presented concerted proton transfer mechanism requires a specific molecular organisation of the water molecules. Figure 8 (bottom left) monitors the N-H_1, N-H_2 and O_g-$H_{3,X}$ bond distances for a trajectory leading to glycine anion in a cluster with 27 water molecules. At 1.9 ps, the carboxilic proton is transfered to a water molecule but, contrary to the Z-Gly form, this proton remains attached on a water molecule and no N-H bond is formed after 10ps.

Similarly to the dynamics of the neutral and zwitterion glycine forms, a rotamer configuration was also observed for the glycine anion (see Figure 5-bottom left).

3.1.4 Hydrogen delocalisation patterns

The last glycine form observed in the dynamics consists in a proton delocalisation in between the carboxylic functional group of glycine and one (or two) water molecules. The carboxilic hydrogen is shared between two oxygen atoms, namely that of the closest water molecule and the one to which it was initially bonded (see Figure 7-bottom left). Sometimes, the hydrogen atom remains at equal distance between the two oxygen atoms (see Figure 8-bottom right capture at t=2.9ps), whereas, in some others, it oscillates between two oxygen atoms (see Figure 8-bottom right - snapshots at t=4.0ps and t=10.0ps). Proton delocalised glycine can be defined as an oscillation between an unstable anion and a neutral glycine forms. The interchanging of H proton and bond formation at different stages of the dynamics is illustrated in Figure 8 (bottom right) which shows the crossing curves corresponding to O_g-$H_{3,X}$ and O_w-$H_{3,X}$ distances where O_g and O_w are the involved oxygen atoms on the glycine and water molecules, respec-

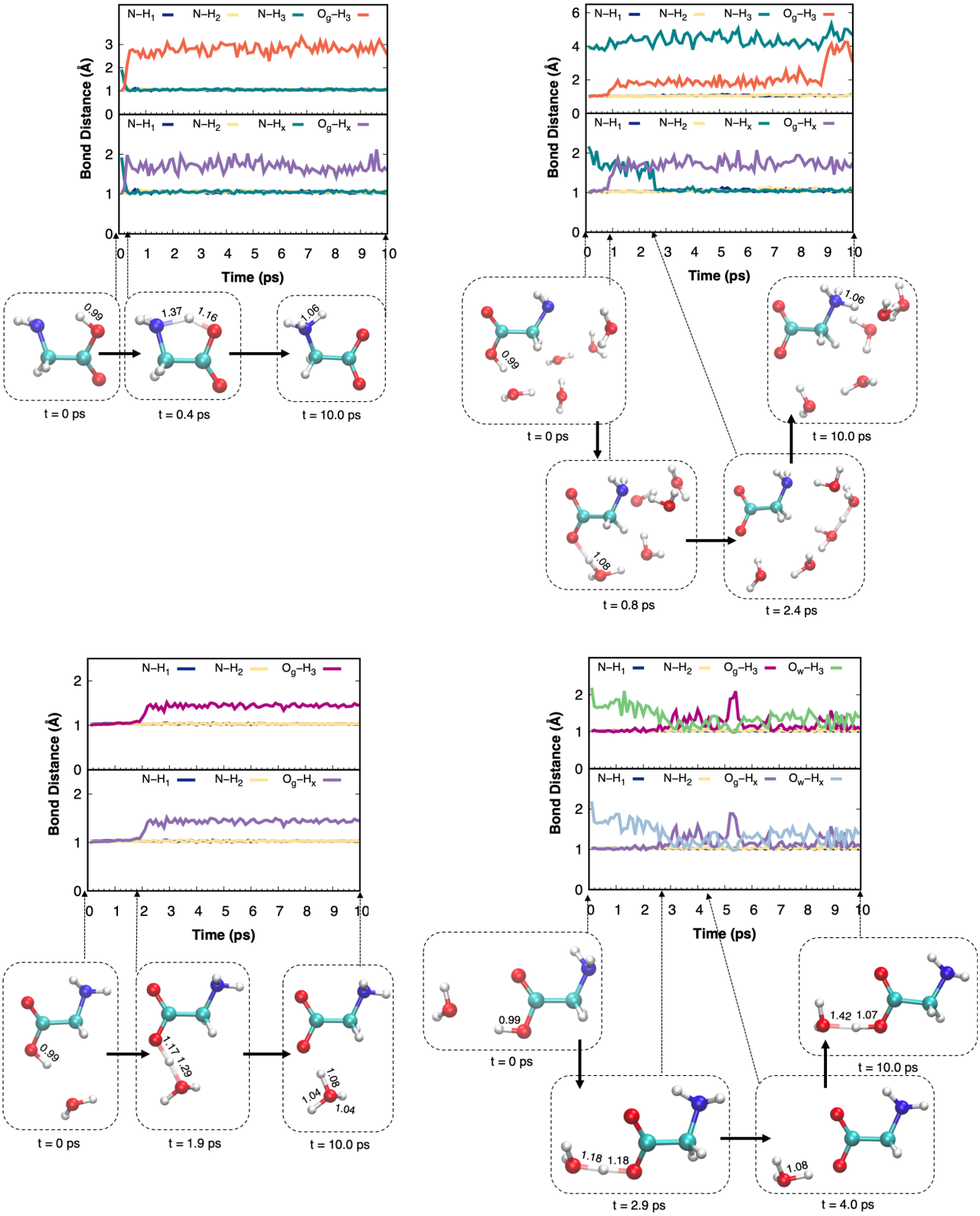

Fig. 8 Snapshots and time evolution of characteristic bond distances for four different transformation mechanisms leading to zwitterion, with direct (top left) or concerted (top right) mechanisms, anion (bottom left) or H-delocalised (bottom right) forms extracted from clusters simulations. Top left: *cc*-Gly-27H_2O (T=250K); top right: tc-Gly-27H_2O (T=250K); bottom left: tc-Gly-27H_2O (T=20K); bottom right: *tt*-Gly-17H_2O (T=250K). O_g and O_w refer to glycine or water oxygen atoms. H_1 and H_2 (resp. H_3) identify the protons which, at $t = 0$ps, belong to the amino (resp. carboxylic) group. At each time, O_g-H_x (resp. O_w-H_x) is the closest distance between any proton and any of the carboxylic oxygen (resp. water oxygen) atom whereas N-H_x is the third closest distance between the nitrogen atom and any proton.

tively, and O_w-H_X is the distance between O_w and its third closest hydrogen atom. Very rarely, a mechanism with two delocalised protons could be identified during the dynamics (see Figure 7-bottom right). The dehydrogenation of one of the carboxylic oxygen atom is rapidly followed by the hydrogenation of the other one, in a concerted hydrogen transfer mechanism through the water environment. This double dehydrogenation / hydrogenation mechanisms occurs several times along the trajectories. Similarly to the anionic glycine form, the proton delocalisation patterns were observed only in dynamics with initial *ct*-, *tc*- and *tt*-N-Gly isomers. Due to the proximity of the two functional groups in *cc*-N-Gly isomer, N-Gly $\rightarrow$ Z-Gly transformation is favourable and prevents the hydrogen delocalisation.

Finally, identically to previous glycine forms, a proton delocalised rotamer was observed in some dynamics as illustrated in Figure 5 (bottom right).

Anionic or poton-delocalized intermediates or transition state structures were not considered, to the best of our knowledge, in mechanistic studies of glycine tautomerization reactions. Let us finally mention, that addressing the proton delocalisation character[69,70] would in principle require a quantum treatment of hydrogen atoms, for instance making use of Path Integral MD schemes[71,72]. These latter studies are beyond the scope of the present work.

3.2 Effect of water environement complexity vs system temperature

In this section, we address the dependence on the temperature and the size of the water environment of the various *xy*-N-Gly-nH_2O and *xy*-N-Gly-LDA structural transformations, reported in the previous section. The results of the molecular dynamics simulations at T=20, 250 and 450K for 3ps and their continuations until 10ps are gathered in Figure 9-A and -B. We mention that, in the case of the simulations with the LDA ice model, only one out of four trajectories achieved at 3ps could be continued up to 10ps due to computational cost. The latter were taken among those which did not show any transformation in the simulated first 3ps. For convenience, we will call in the following the water clusters of different sizes as: (i) small clusters to refer to clusters with n=4 H_2O molecules; (ii) intermediate clusters to refer to clusters with n=17 and 27 water molecules and (iii) LDA ice to refer to the largest model (343-344 water molecules).

We first discuss the dynamical evolution of the *cc*-N-Gly isomer. In Figure 9-A and B upper panels, the initial neutral *cc*-N-Gly geometry was maintained in some trajectories while the tautomerization toward a Z-Gly form was observed in the trajectories of other replicas (see Section 3.1.2). The latter occurs most frequently through a direct proton transfer. The formation of Z-Gly conformer was observed often (of about 75 and 100 %) in the intermediate cluster sizes, at the three temperatures (light blue histogram columns in Figure 9-upper panel at both 3 and 10ps). In the case of the LDA ice model, the zwitterionic form appears in 25 % at T=20 and 250K, whereas higher temperatures (T=450K) favoured the Z-Gly tautomerization.

The following common features were captured for trajectories with initial *tt*-, *ct*- and *tc*-N-Gly-nH_2O(LDA) structures (Figure 9-A and -B middle and lower panel). For all the small clusters, glycine molecules remained practically in their neutral forms whatever the temperature, the initial isomer structure and the simulation length (3 or 10ps). Indeed, in these small systems, the water network is insufficient to completely surround the glycine molecules, which limits the transformation possibilities. This is in line with recent studies on the free-energy surfaces at 300K with biased meta-dynamics simulations, demonstrating that the zwitterionic form in Gly$(H_2O)_4$ cluster is unstable[73].

Furthermore, in the intermediate cluster sizes all the transformations reported in Section 3.1 can be observed, namely anion (Fig. 9 orange columns), proton delocalisation (red) and zwitterion glycine. When N-Gly tautomerization toward Z-Gly form was observed, it was in every cases due to a concerted proton mechanism. This is in line with the frequent observations of anion and proton delocalization glycine forms, as these patterns can be seen as preliminary forms for such concerted mechanism. It can be extrapolated that in longer dynamics (> 10ps) Z-Gly tautomerization might take place. Surprisingly, N-Gly form is seen to be always maintained at the highest 450K temperature. This can be explained by the fact that glycine molecule moves from the cluster's center toward its borders. Indeed, the water molecules preferred to build a hydrogen-bond network between them by displacing the glycine molecule toward clusters borders, where the water coordination effect is smaller and therefore less favourable to chemical transformations of glycine. Note that for the cases of *ct*- and *tc*-N-Gly isomers, the migrations of glycine toward the clusters' borders was often associated with a conformer transformation (*ct* $\rightarrow$ *tt* or *tc* $\rightarrow$ *cc*).

On the other hand, in the ice representative model, such a glycine migration toward the surface was not observed due to the larger number of water shells around the glycine system. Rearrangements of water molecules in this system did not occur because the hydrogen-bond network between the water molecules in the outer solvation shells of glycine was already formed, at variance to the small and intermediate sizes models. Therefore, in *tt*-, *ct*- and *tc*-N-Gly-LDA ice molecular systems, the glycine molecule remains neutral in all simulations at 20 K and 250 K. At 450K, proton delocalization patterns are observed. Note that these proton delocalisation patterns were also sometime observed on very short and limited periods in some trajectories denoted as "Neutral", because such transfers were not representative of the overall trajectory. This points out to the unstable character of proton delocalization form in these cases.

When comparing series of simulations at both, 3ps (Fig.9-A) and 10ps (Figure 9-B), it appears that trajectories characterized as proton delocalisation up to 3ps, were latter on identified as anion forms until the end of the 10ps dynamics. The opposite transformations (from anion to proton delocalised) were also observed. The oscillations between these two unstable forms, even for the anion conformer, can be explained by the proton proximity. The proton originally attached to the carboxilic functional group, remains unbounded but close to the carboxylic group. Similarly, considering simulations only up to 3ps, some proton delocalization forms were identified and latter stabilized toward the neutral

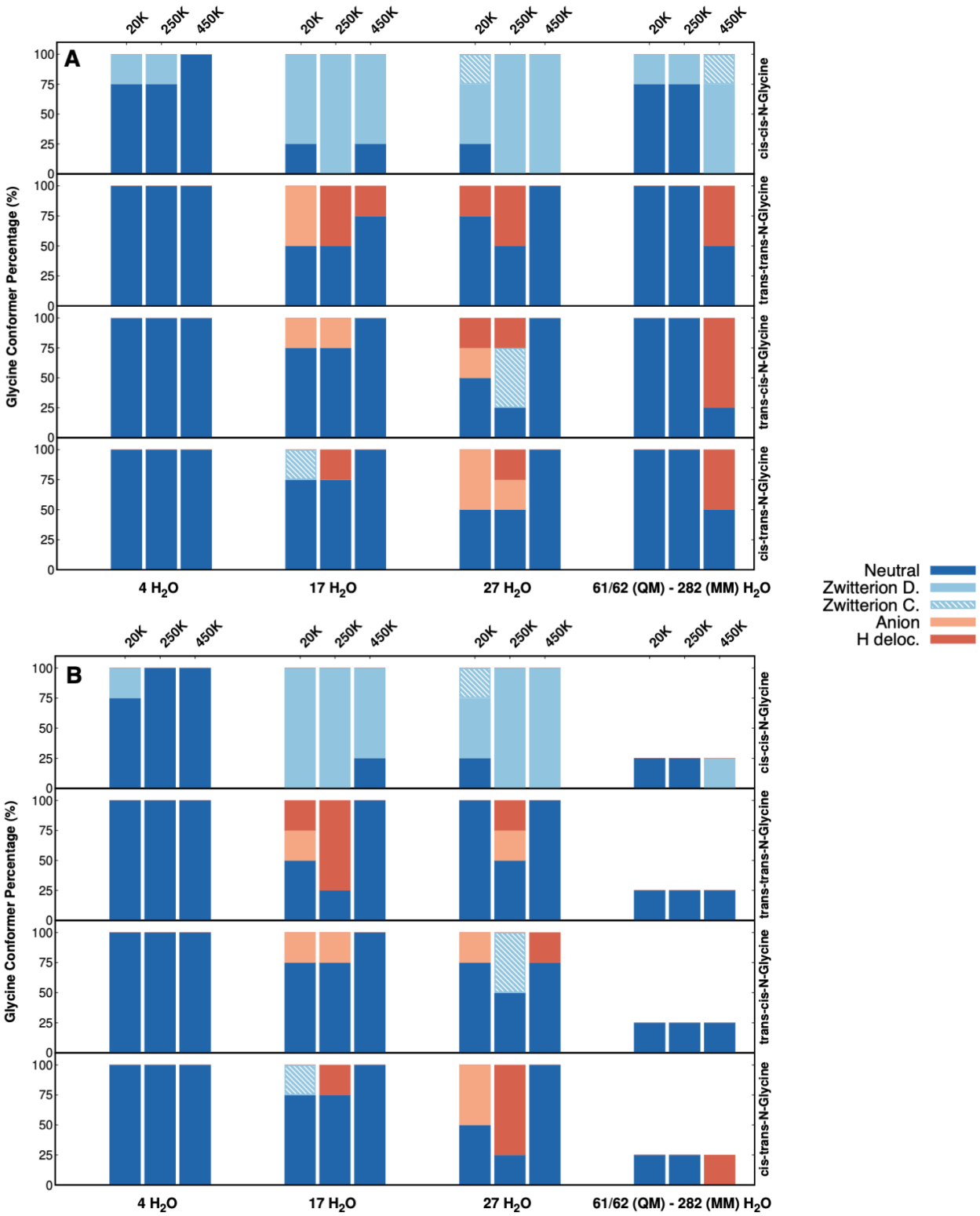

Fig. 9 Dominant glycine transformations observed during the first part (3ps, top A) and full part of trajectories (10ps, bottom B) differing by the initial isomer, its initial localisation, the number of water molecules and the temperature. For the largest systeme (LDA ice), a single simulation was performed up to 10ps per isomer/size/temperature due to the great computational time requirements.

form. This points out the importance of the length of the trajectories to discuss the tautomerization of glycine in water.

4 Summary and conclusion

In this study QM/MM molecular dynamic simulations at three different temperatures, namely T=20, 250 and 450 K, were carried out starting from four different neutral glycine isomers (*cc*, *ct*, *tc*, *tt*) immersed in water clusters of various sizes (n=4, 17, 27 H_2O molecules) and a large-size LDA ice representative model (343-344 H_2O molecules). We analysed glycine conformations explored during the trajectories up to 10ps.

The following general trends were identified : (i) in the ice representative models, the neutral glycine is stabilized at 20 K and 250 K, but not at the high temperature (450K). In the latter case, the tautomerization transformation towards Z-Gly form were mostly observed for the *cc*-N-Gly-LDA, whereas for the other isomers proton delocalization forms were observed. (ii) The trends reported in the ice representative model, and in particular the tautomerization, can only be observed when explicitly considering the large water network around glycine, the simulations with a smaller number of water molecules leading to different conclusions. In the case of n = 4, 17 and 27 H_2O clusters, the glycine solvation shell tends to disappear because of the water hydrophilic character, which favours the aggregation of water molecules between them, thus displacing the glycine toward cluster borders. Consequently, some of the glycine functional groups (carboxilic or amino) remain unbounded to water, which stabilizes the N-Gly conformer. This is well evidenced for the case of small (-4H_2O) cluster. Even at high temperatures (T=450K), the lack of water embedding the glycine molecule prevents the transformation to Z-Gly. This is consistent with previous free energy studies that evidenced the stabilization of neutral glycine in gas phase or surrounded by few water molecules[25,34,73]. (iii) With sufficient number of molecules, the efficiency of the tautomerisation process (N-Gly $\rightarrow$ Z-Gly) depends on the nature of the glycine isomers. This is also the case of the associated mechanism. For instance the direct mechanism occurred only from the *cc*-N-GlynH2O isomers, whereas for *ct*- and *tc*-N-Gly molecular systems, the proton transfer was assisted by the water molecules in a concerted mechanism.

This work enforces the idea that considering the various glycine isomers is mandatory to provide a complete picture of the tautomerisation mechanisms. In addition to the initial isomers structures, the other factor driving the tautomerization is the representation of the water environment. Both water and glycine dynamics are also temperature dependent. For intermediate size clusters, water - water aggregation occurs faster at T = 450K, which stabilises N-Gly. At this temperature and in the large size water model (starting from LDA-ice model), *cc*-N-Gly is fully converted to Z-Gly, whereas for the other three isomers, the delocalisation between H_2O and -COO- group dominates.

In addition, we demonstrated that the glycine tautomerization process is strongly influenced by the nature of its conformational isomer. The Z-Gly isomer is relatively rapidly formed from *cc*-N-Gly predominantly via a direct H-transfer, whereas the *ct*-, *tc*- and *tt*-N-Gly isomers undergo different transformations such as anion and proton delocalised forms.

From the stand point of chemical simulations, comparing LDA-ice and smaller clusters calculations strongly suggests that modeling interstellar bulk chemistry requires few water layers (our LDA ice model) surrounding the reactants to avoid self-aggregation of the water molecules.

From the stand point of Astrochemistry, our study suggests that glycine in the cold interstellar ices should remain neutral up to at least 250K. These results can be compared with the experimental works of Ioppolo *e*t al.[16] where glycine molecules remain mostly neutral at T smaller than 240 K. Maté *et al.*[19] reported the N$\rightarrow$ Z tautomerization transformation in a polar (water) medium at $\sim$25 K. These apparent discrepancies may be due to differences in the experimental set-up. In the latter work, glycine is vapor-deposited on a cold substrate and then heated up to the desired temperature to perform FTIR measurements, whereas in the work of Ioppolo *et al.*[16] glycine is formed in a neutral form and monitored by in-situ RAIR experiments. Our simulations are therefore closer to the experimental conditions in the work of Ioppolo *et al.* who reported that glycine is formed mainly in its neutral form in interstellar ice and that heating the system resulted in the loss of neutral glycine isomer's spectral signature, and the appearance of zwitterionic glycine one. This is in line with our ice-model simulations, where transformations toward zwitterionic or H-delocalized forms are favored when increasing the temperature above 250 K.

Finally, the evolution of a glycine molecule surrounded by few water molecules (intermediate clusters) was also simulated. These simulations provide several hints on the understanding of various processes occurring in the ice-surface vicinity, namely the sublimation of ices and its compounds, for instance in the coma of comets[10,41,74].

5 Supplementary information

Authors contributions

MYB wrote the draft and carried out dynamics simulations, TM edited the draft and carried out part of the dynamics simulations, MR and DT edited the draft, TM and MR supervised the project; the manuscript was written with contribution from all the co-authors. All the co-authors read and approved the manuscript.

Conflicts of interest

There are no conflicts to declare.

Acknowledgements

All authors acknowledge the Agence Nationale de la Recherche (ANR) (project ANR-19-CE29-0011-02 RUBI). TM acknowledges the access to the HPC resources of CCRT/CINES/IDRIS, which was granted under the allocation A0130807369 by GENCI. MYB and MR acknowledge HPC mesocenter CALMIP (UAR CNRS 3667) for allocation of computer resources (p0059 and p18009).

Notes and references

1 K. Kvenvolden, J. Lawless, K. Pering, E. Peterson, J. Flores, C. Ponnamperuma, I. Klapan and C. Moore, Nature, 1970, **228**, 923–926.

2 J. E. Elsila, D. P. Glavin and J. P. Dworkin, Meteoritics & Planetary Science, 2009, **44**, 1323–1330.

3 K. Altwegg, H. Balsiger, A. Bar-Nun, J.-J. Berthelier, A. Bieler, P. Bochsler, C. Briois, U. Calmonte, M. R. Combi, H. Cottin, J. D. Keyser, F. Dhooghe, B. Fiethe, S. A. Fuselier, S. Gasc, T. I. Gombosi, K. C. Hansen, M. Haessig, A. Jäckel, E. Kopp, A. Korth, L. L. Roy, U. Mall, B. Marty, O. Mousis, T. Owen, H. Rème, M. Rubin, T. Sémon, C.-Y. Tzou, J. H. Waite and P. Wurz, Science Advances, 2016, **2**, e1600285.

4 E. T. Parker, H. L. McLain, D. P. Glavin, J. P. Dworkin, J. E. Elsila, J. C. Aponte, H. Naraoka, Y. Takano, S. Tachibana, H. Yabuta, H. Yurimoto, K. Sakamoto, T. Yada, M. Nishimura, A. Nakato, A. Miyazaki, K. Yogata, M. Abe, T. Okada, T. Usui, M. Yoshikawa, T. Saiki, S. Tanaka, S. Nakazawa, Y. Tsuda, F. Terui, T. Noguchi, R. Okazaki, S. ichiro Watanabe and T. Nakamura, Geochimica et Cosmochimica Acta, 2023, **347**, 42–57.

5 C. Ceccarelli, L. Loinard, A. Castets, A. Faure and B. Lefloch, Astronomy and Astrophysics, 2000, **362**, 1122–1126.

6 Y.-J. Kuan, S. B. Charnley, H.-C. Huang, W.-L. Tseng and Z. Kisiel, The Astrophysical Journal, 2003, **593**, 848.

7 L. E. Snyder, F. J. Lovas, J. M. Hollis, D. N. Friedel, P. R. Jewell, A. Remijan, V. V. Ilyushin, E. A. Alekseev and S. F. Dyubko, The Astrophysical Journal, 2005, **619**, 914.

8 E. Herbst, Chem. Soc. Rev., 2001, **30**, 168–176.

9 R. T. Garrod, The Astrophysical Journal, 2013, **765**, 60.

10 K. Hadraoui, H. Cottin, S. Ivanovski, P. Zapf, K. Altwegg, Y. Benilan, N. Biver, V. Della Corte, N. Fray, J. Lasue et al., Astronomy & Astrophysics, 2019, **630**, A32.

11 S. A. Krasnokutski, C. Jäger and T. Henning, The Astrophysical Journal, 2020, **889**, 67.

12 G. M. Muñoz Caro, U. J. Meierhenrich, W. A. Schutte, B. Barbier, A. Arcones Segovia, H. Rosenbauer, W. H. P. Thiemann, A. Brack and J. M. Greenberg, Nature, 2002, **416**, 403–406.

13 P. D. Holtom, C. J. Bennett, Y. Osamura, N. J. Mason and R. I. Kaiser, The Astrophysical Journal, 2005, **626**, 940.

14 J. E. Elsila, J. P. Dworkin, M. P. Bernstein, M. P. Martin and S. A. Sandford, The Astrophysical Journal, 2007, **660**, 911.

15 C.-W. Lee, J.-K. Kim, E.-S. Moon, Y. C. Minh and H. Kang, The Astrophysical Journal, 2009, **697**, 428.

16 S. Ioppolo, G. Fedoseev, K. J. Chuang, H. M. Cuppen, A. R. Clements, M. Jin, R. T. Garrod, D. Qasim, V. Kofman, E. F. van Dishoeck and H. Linnartz, Nature Astronomy, 2021, **5**, 197–205.

17 S. Maclot, D. G. Piekarski, A. Domaracka, A. Méry, V. Vizcaino, L. Adoui, F. Martín, M. Alcamí, B. A. Huber and P. Rousseau, The Journal of Physical Chemistry Letters, 2013, **4**, 3903–3909.

18 S. Maclot, D. G. Piekarski, R. Delaunay, A. Domaracka, A. Méry, V. Vizcaino, J.-Y. Chesnel, F. Martín, M. Alcamí, B. A. Huber, L. Adoui, P. Rousseau and S. Díaz-Tendero, The European Physical Journal D, 2014, **68**, 149.

19 B. Maté, Y. Rodriguez-Lazcano, Ó. Gálvez, I. Tanarro and R. Escribano, Phys. Chem. Chem. Phys., 2011, **13**, 12268–12276.

20 K. Iijima, K. Tanaka and S. Onuma, Journal of Molecular Structure, 1991, **246**, 257–266.

21 R. M. Balabin, Chemical Physics Letters, 2009, **479**, 195–200.

22 P. D. Godfrey and R. D. Brown, Journal of the American Chemical Society, 1995, **117**, 2019–2023.

23 C. H. Hu, M. Shen and H. F. Schaefer III, Journal of the American Chemical Society, 1993, **115**, 2923–2929.

24 O. Rahaman, A. C. T. van Duin, W. A. I. Goddard and D. J. Doren, The Journal of Physical Chemistry B, 2011, **115**, 249–261.

25 B. Balta and V. Aviyente, Journal of Computational Chemistry, 2003, **24**, 1789–1802.

26 G. M. Chaban and R. B. Gerber, The Journal of Chemical Physics, 2001, **115**, 1340–1348.

27 I. Tuñón, E. Silla and M. F. Ruiz-López, Chemical Physics Letters, 2000, **321**, 433–437.

28 N. Kishimoto, Chemical Physics Letters, 2017, **667**, 172–179.

29 J. Sun, D. Bousquet, H. Forbert and D. Marx, The Journal of Chemical Physics, 2010, **133**, 114508.

30 M. Haranczyk and M. Gutowski, The Journal of Chemical Physics, 2008, **128**, 125101.

31 C. K. Kim, B.-H. Park, H. W. Lee and C. K. Kim, Organic & Biomolecular Chemistry, 2013, **11**, 1407–1413.

32 F. R. Tortonda, J. L. Pascual-Ahuir, E. Silla and I. Tuñón, Journal of Molecular Structure: THEOCHEM, 2003, **623**, 203–210.

33 R. Ramaekers, J. Pajak, B. Lambie and G. Maes, The Journal of Chemical Physics, 2004, **120**, 4182–4193.

34 M. K. Ghosh, T. H. Choi and C. H. Choi, Theoretical Chemistry Accounts, 2016, **135**, 103.

35 Q. Cui, The Journal of Chemical Physics, 2002, **117**, 4720–4728.

36 S. Tolosa, A. Hidalgo and J. A. Sansón, Journal of Molecular Modeling, 2014, **20**, 2147.

37 S. M. Bachrach, The Journal of Physical Chemistry A, 2008, **112**, 3722–3730.

38 M. Nagaoka, N. Okuyama-Yoshida and T. Yamabe, The Journal of Physical Chemistry A, 1998, **102**, 8202–8208.

39 S. Tolosa, A. Hidalgo and J. A. Sansón, The Journal of Physical Chemistry B, 2012, **116**, 13033–13044.

40 H. Miyamoto and M. Aida, Chemistry Letters, 2013, **42**, 598–600.

41 C. R. Arumainayagam, R. T. Garrod, M. C. Boyer, A. K. Hay, S. T. Bao, J. S. Campbell, J. Wang, C. M. Nowak, M. R. Arumainayagam and P. J. Hodge, Chemical Society Reviews, 2019, **48**, 2293–2314.

42 A. Koster, G. Geudtner, A. Alvarez-Ibarra, P. Calaminici, M. Casida, J. Carmona-Espindola, V. Dominguez, R. Flores-Moreno, G. Gamboa, A. Goursot, T. Heine, A. Ipatov, A. de la Lande, F. Janetzko, J. del Campo, D. Mejia-Rodriguez, J. U. Reveles, J. Vasquez-Perez, A. Vela, B. Zuniga-Gutierrez and D. Salahub, deMon2k Version 6, 2018.

43 N. Godbout, D. R. Salahub, J. Andzelm and E. Wimmer,

Canadian Journal of Chemistry, 1992, **70**, 560–571.
44 R. Flores-Moreno and J. V. Ortiz, The Journal of Chemical Physics, 2009, **131**, 124110.
45 J. P. Perdew, K. Burke and M. Ernzerhof, Physical Review Letters, 1996, **77**, 3865–3868.
46 A. Rimola, N. Balucani, C. Ceccarelli and P. Ugliengo, International Journal of Molecular Sciences, 2022, **23**, year.
47 W. Xu, Q. Zhu and C. T. Hu, Angewandte Chemie International Edition, 2017, **56**, 2030–2034.
48 A. Goursot, T. Mineva, R. Kevorkyants and D. Talbi, Journal of Chemical Theory and Computation, 2007, **3**, 755–763.
49 A. de la Lande, A. Alvarez-Ibarra, K. Hasnaoui, F. Cailliez, X. Wu, T. Mineva, J. Cuny, P. Calaminici, L. López-Sosa, G. Geudtner, I. Navizet, C. Garcia Iriepa, D. R. Salahub and A. M. Köster, Molecules, 2019, **24**, year.
50 V. Hornak, R. Abel, A. Okur, B. Strockbine, A. Roitberg and C. Simmerling, Proteins: Structure, Function, and Bioinformatics, 2006, **65**, 712–725.
51 W. D. Cornell, P. Cieplak, C. I. Bayly, I. R. Gould, K. M. Merz, D. M. Ferguson, D. C. Spellmeyer, T. Fox, J. W. Caldwell and P. A. Kollman, Journal of the American Chemical Society, 1995, **117**, 5179–5197.
52 W. S. Ross and C. C. Hardin, Journal of the American Chemical Society, 1994, **116**, 6070–6080.
53 J. Åqvist, The Journal of Physical Chemistry, 1990, **94**, 8021–8024.
54 C. G. BROYDEN, IMA Journal of Applied Mathematics, 1970, **6**, 76–90.
55 R. Fletcher, The Computer Journal, 1970, **13**, 317–322.
56 D. Goldfarb, Mathematics of Computation, 1970, **24**, 23–26.
57 D. F. Shanno, Mathematics of Computation, 1970, **24**, 647–656.
58 S. Nosé, J. Chem. Phys., 1984, **81**, 511.
59 W. G. Hoover, Phys. Rev. A, 1985, **31**, 1695–1697.
60 A. F. Oliveira, P. Philipsen and T. Heine, J. Chem. Theo. Comp., 2015, **11**, 5209–5218.
61 P. Ghesquière, T. Mineva, D. Talbi, P. Theulé, J. A. Noble and T. Chiavassa, Physical Chemistry Chemical Physics, 2015, **17**, 11455–11468.
62 D. Van Der Spoel, E. Lindahl, B. Hess, G. Groenhof, A. E. Mark and H. J. C. Berendsen, Journal of Computational Chemistry, 2005, **26**, 1701–1718.
63 H. J. Fraser, M. P. Collings, M. R. S. McCoustra and D. A. Williams, Monthly Notices of the Royal Astronomical Society, 2001, **327**, 1165–1172.
64 E. Kassab, J. Langlet, E. Evleth and Y. Akacem, Journal of Molecular Structure: THEOCHEM, 2000, **531**, 267–282.
65 P. Bandyopadhyay, M. S. Gordon, B. Mennucci and J. Tomasi, The Journal of Chemical Physics, 2002, **116**, 5023–5032.
66 C.-K. Kim, B.-H. Park, H.-W. Lee and C.-K. Kim, Bulletin of the Korean Chemical Society, 2011, **32**, 1985–1992.
67 S. Pilling, L. A. Mendes, V. Bordalo, C. F. Guaman, C. R. Ponciano and E. F. da Silveira, Astrobiology, 2013, **13**, 79–91.
68 D. Guerra, L. A. Gomez, A. Restrepo and J. David, Chemical Physics, 2020, **530**, 110645.
69 L. Wang, S. D. Fried, S. G. Boxer and T. E. Markland, Proceedings of the National Academy of Sciences, 2014, **111**, 18454–18459.
70 F. Louisnard, T. Mineva and J. Cuny, Theoretical Chemistry Accounts, 2022, **141**, 36.
71 D. Marx and M. Parrinello, Zeitschrift für Physik B Condensed Matter, 1994, **95**, 143–144.
72 S. Habershon, B. J. Braams and D. E. Manolopoulos, The Journal of chemical physics, 2007, **127**, year.
73 R. Tripathi, L. Durán Caballero, R. Pérez de Tudela, C. Hölzl and D. Marx, ACS omega, 2021, **6**, 12676–12683.
74 R. T. Garrod, M. Jin, K. A. Matis, D. Jones, E. R. Willis and E. Herbst, The Astrophysical Journal Supplement Series, 2022, **259**, 1.